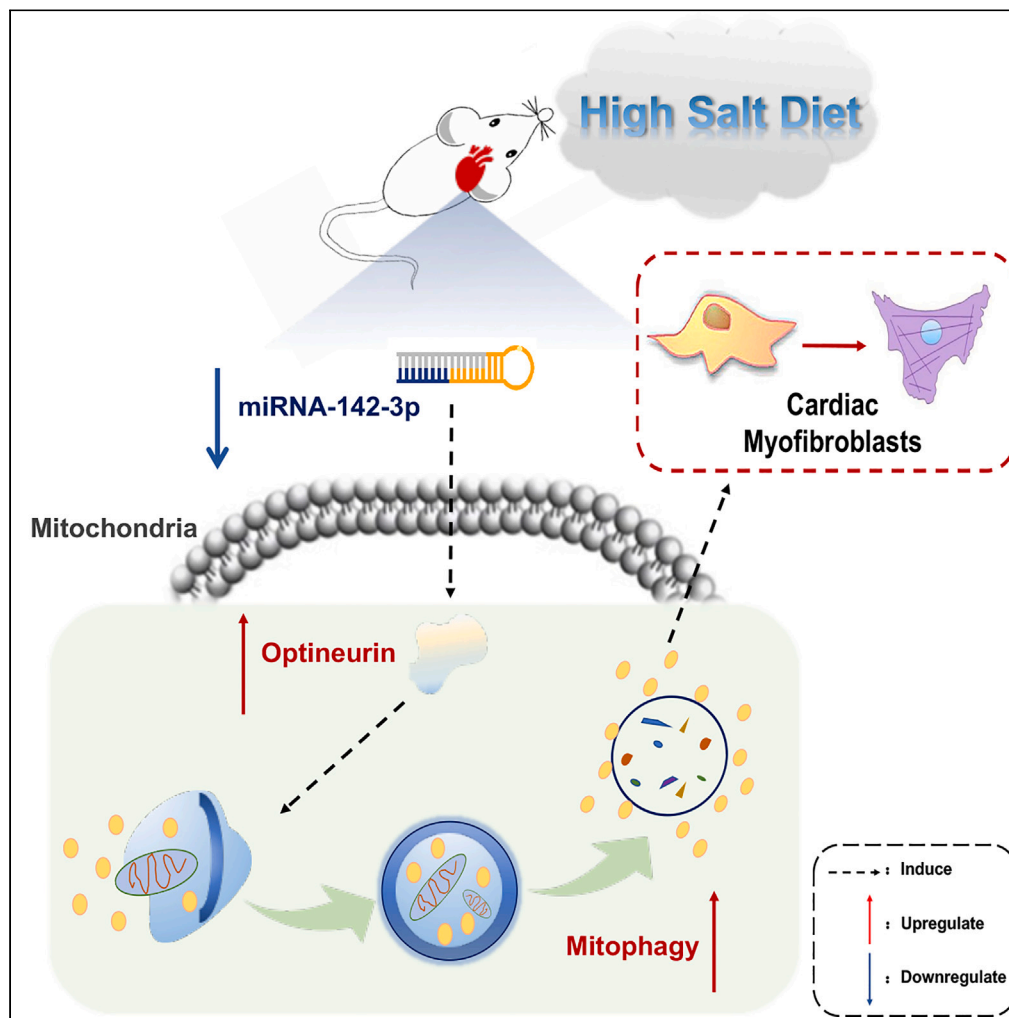


Article

MicroRNA-142-3p alleviated high salt-induced cardiac fibrosis via downregulating optineurin-mediated mitophagy



Yong Li, Kun Zhao, Yifang Hu, Fengze Yang, Peng Li, Yun Liu

liyongmydream@126.com (Y.L.)
lipeng198610@163.com (P.L.)
liuyun@njmu.edu.cn (Y.L.)

Highlights

Upregulated miR-142-3p could mitigate high salt-induced cardiac fibrosis

Optineurin (OPTN) was increased in the mitochondria of NaCl-induced NRCF

OPTN-mediated mitophagy was involved in anti-cardiac fibrosis effects of miR-142-3p

Li et al., iScience 27, 109764
May 17, 2024 © 2024 The Authors. Published by Elsevier Inc.
<https://doi.org/10.1016/j.isci.2024.109764>



Article

MicroRNA-142-3p alleviated high salt-induced cardiac fibrosis via downregulating optineurin-mediated mitophagy

Yong Li,^{1,2,6,7,*} Kun Zhao,^{1,6} Yifang Hu,³ Fengze Yang,¹ Peng Li,^{1,*} and Yun Liu^{4,5,*}

SUMMARY

High salt can induce cardiac damage. The aim of this present study was to explore the effect and the mechanism of microRNA (miR)-142-3p on the cardiac fibrosis induced by high salt. Rats received high salt diet to induce cardiac fibrosis *in vivo*, and neonatal rat cardiac fibroblasts (NRCF) treated with sodium chloride (NaCl) to induce fibrosis *in vitro*. The fibrosis and mitochondrial autophagy levels were increased the heart and NRCF treated with NaCl, which were alleviated by miR-142-3p upregulation. The fibrosis and mitochondrial autophagy levels were elevated in NRCF after treating with miR-142-3p antagomiR. Optineurin (OPTN) expression was increased in the mitochondria of NRCF induced by NaCl, which was attenuated by miR-142-3p agomiR. OPTN downregulation inhibited the increases of fibrosis and mitochondrial autophagy levels induced by NaCl in NRCF. These results miR-142-3p could alleviate high salt-induced cardiac fibrosis via downregulation of OPTN to reduce mitophagy.

INTRODUCTION

Excessive sodium intake is associated with the development of a variety of comorbidities including chronic kidney disease, liver disease, neurological disease, and cardiovascular diseases.^{1–3} High sodium intake can lead to cardiovascular diseases such as hypertension, cardiac remodeling, and myocardial apoptosis.^{4,5} Salt sensitivity of blood pressure varies widely between individuals and there are data suggesting that salt adversely affects heart, irrespective of blood pressure.⁶

Autophagy is a catabolic process involved in maintaining energy and organelle homeostasis.⁷ Autophagy contributes to the maintenance of cardiac homeostasis, and the level of autophagy is dynamically altered in heart disease.^{8,9} Mitophagy, which mediates the selective elimination of dysfunctional mitochondria, is essential for cardiac homeostasis.¹⁰ In cardiomyocytes, mitophagy is closely associated with metabolic activity, cell differentiation, apoptosis, and other physiological processes involved in major phenotypic alterations.¹¹ Previous study showed that mitophagy is a mechanism counteracting the high-salt-induced oxidative stress-related organ damage.¹² We presently will explore the mitophagy in the roles of cardiac fibrosis induced by high salt diet (HSD).

Optineurin (OPTN) is a multifunctional adaptor protein intimately involved in various vesicular trafficking pathways.¹³ The OPTN protein is a selective autophagy receptor (or adaptor), containing an ubiquitin binding domain with the ability to bind polyubiquitinated cargoes and bring them to autophagosomes via its microtubule-associated protein 1 light chain 3-interacting domain.^{14,15} Previous studies have reported that silencing OPTN could ameliorate LPS-induced or high-glucose (HG)-induced mitophagy in renal tubular epithelial cells (RTECs), suggesting the vital regulatory role of OPTN-mediated mitophagy in the pathological development of diseases.^{16,17} However, the specific effects of OPTN-mediated mitophagy in HSD-induced cardiac fibrosis remained unknown.

MicroRNAs (miRs), a group of small and non-coding RNAs, negatively regulate gene expression via promoting messenger RNA (mRNA) degradation or blocking mRNA translation.¹⁸ Many miRs have been recognized as biomarkers or possible targets for the diagnosis or therapy of some diseases,¹⁹ including cardiovascular diseases.²⁰ Among them, miR-142-3p was involved in the occurrences and progression of various cardiovascular diseases.^{21–23} Previous studies found that miR-142-3p upregulation could ameliorate myocardial ischemia/reperfusion (I/R)-induced transdifferentiation of fibroblasts to myofibroblasts and collagen deposition.^{24,25} Also, in addition to playing a role in the development of various cancers,^{22,26} miR-142-3p-mediated autophagy was reported as a novel mechanism toward I/R-induced cardiac

¹Department of Cardiology, The First Affiliated Hospital of Nanjing Medical University, Nanjing, Jiangsu, China

²Department of Cardiology, The People's Hospital of Qijiang District, Qijiang, Chongqing, China

³Department of Information, The First Affiliated Hospital, Nanjing Medical University, Nanjing, Jiangsu, China

⁴Department of Information, The First Affiliated Hospital, Nanjing Medical University, No.300 Guang Zhou Road, Nanjing, Jiangsu 210029, China

⁵Department of Medical Informatics, School of Biomedical Engineering and Informatics, Nanjing Medical University, Nanjing, Jiangsu 211166, China

⁶These authors contributed equally

⁷Lead contact

*Correspondence: liyongmydream@126.com (Y.L.), lipeng198610@163.com (P.L.), liyun@njmu.edu.cn (Y.L.)

<https://doi.org/10.1016/j.isci.2024.109764>



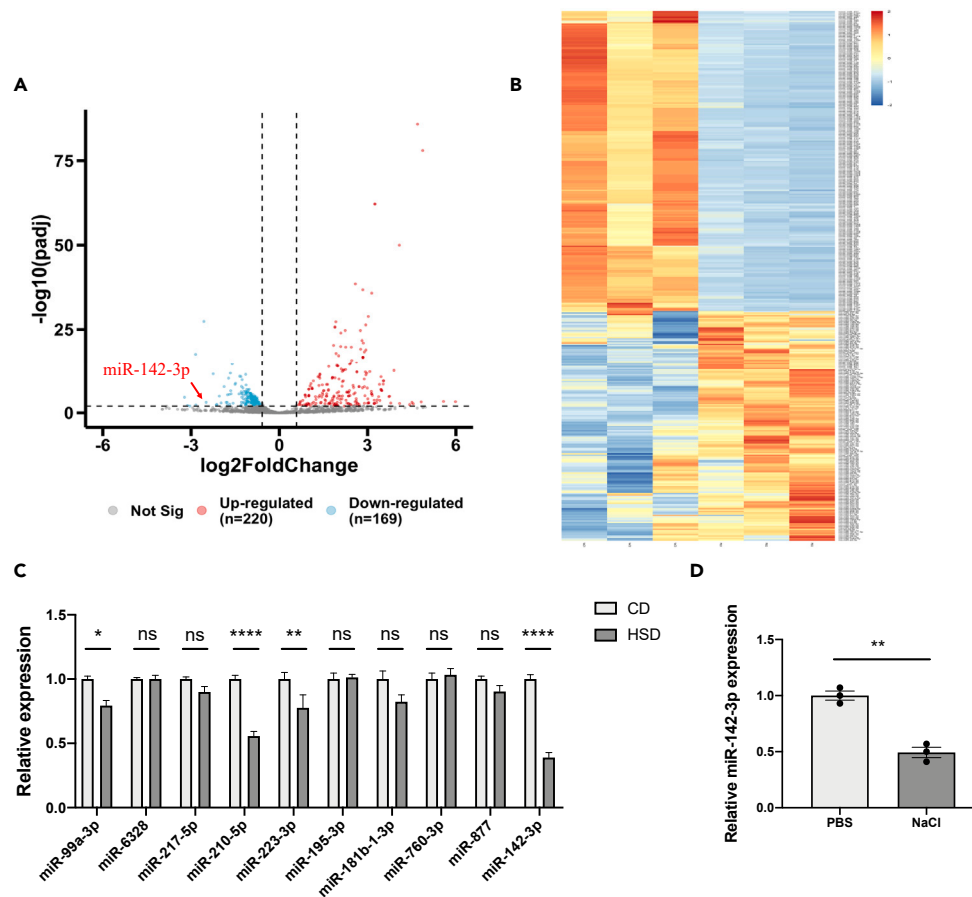


Figure 1. HSD and NaCl downregulated miR-142-3p in vivo and in vitro, respectively

(A and B), The Volcano plot (A) and heatmap (B) visually showed all the detected miRNAs among samples of the two groups.

(C) The top 10 down-regulated miRNAs were quantified by RT-qPCR in the heart tissues.

(D) mRNA expression of miR-142-3p in NRCFs from different groups. $n = 3$ per group, all mRNA and protein expression were normalized to U6. The results are expressed as the mean \pm SEM (* $p < 0.05$, ** $p < 0.01$, *** $p < 0.001$, **** $p < 0.0001$).

injure.^{27,28} Besides, miR-142-3p could mitigate myocardial mitochondrial dysfunction.²⁹ Considering the regulatory role of OPTN in mitochondrial autophagy, it is worth studying whether miR-142-3p could modulate HSD-induced cardiac fibrosis via OPTN-mediated autophagy and mitophagy.

In summary, we supposed that mitophagy was increased in the heart of high salt-treated mice, and this increase resulted in cardiac fibrosis. Upregulation of miR-142-3p alleviated OPTN-mediated mitophagy to reduce cardiac fibrosis induced by high salt.

RESULTS

HSD-induced myocardial fibrosis in vivo and NaCl-induced cardiac fibrosis in vitro

As we previously reported,⁵ HSD induced collagen deposition significantly in the left ventricle of rats compared with those in the normal control (NC) group (Figure S1A), which was also supported by the augmented mRNA and protein expression of collagen I, α -SMA, and TGF- β in the myocardium of rats fed with HSD (Figures S1B and S1C). *In vitro*, 100 mM NaCl increased protein and mRNA expression of collagen I, α -SMA, and TGF- β in NRCFs (Figures S1D and S1E).

HSD and NaCl downregulated miR-142-3p in vivo and in vitro, respectively

Since the vital role of miRNAs-mediated epigenetic regulation in the occurrence and progression of cardiovascular disease (CVD), we performed miRNA-seq in PBS or NaCl-treated NRCFs. In total, 262 upregulated miRNAs and 82 downregulated miRNAs were found. The Volcano plot and Heatmap visually showed all the detected miRNAs among samples of the two groups (Figures 1A and 1B). Next, the top 10 downregulated miRNAs were quantified by RT-qPCR in the heart tissues. Among them, miR-142-3p expression in the heart tissues of HSD

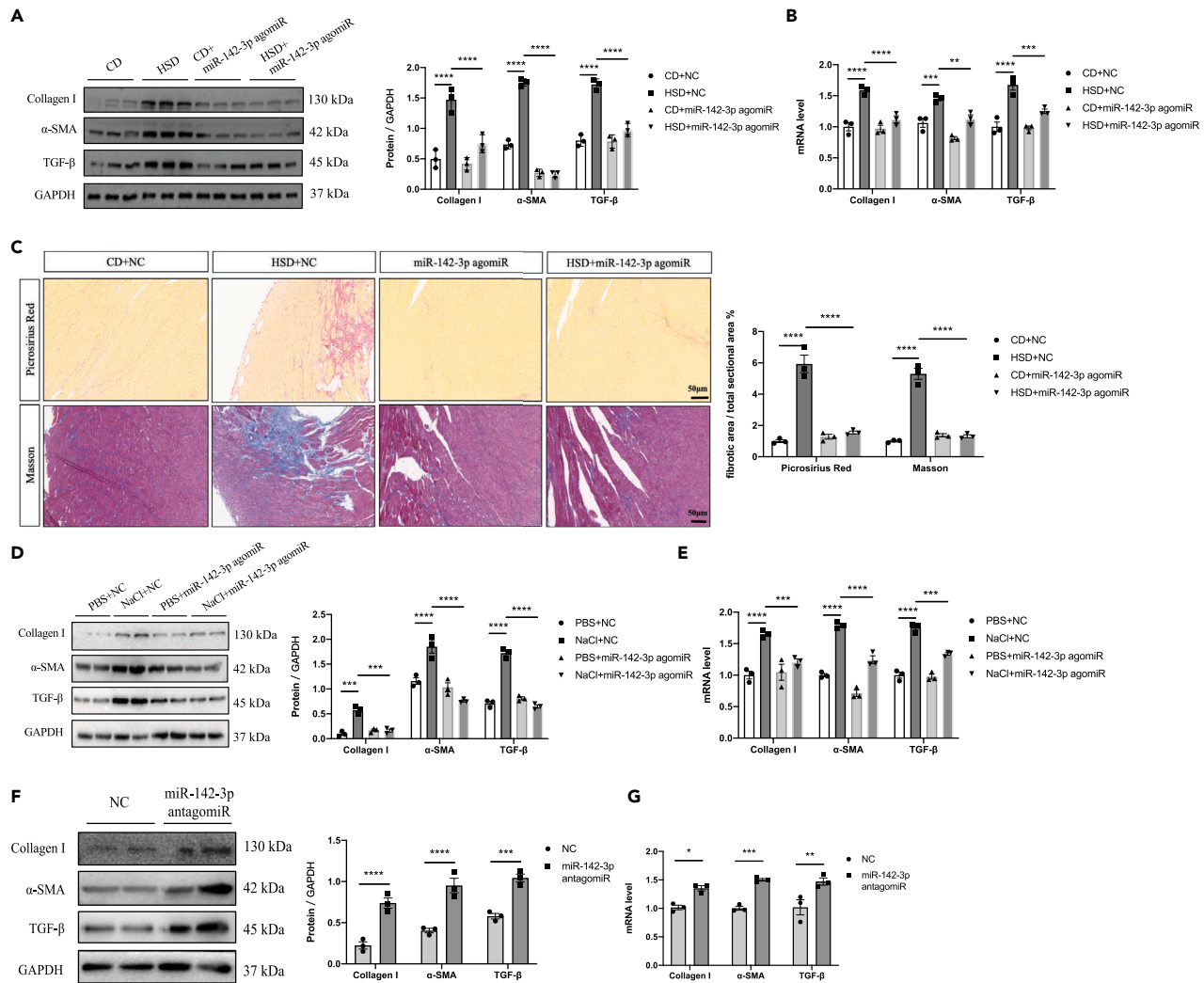


Figure 2. miR-142-3p participated in HSD-induced myocardial fibrosis and NaCl-induced cardiac fibrosis

(A) Protein expression of collagen I, α -SMA, and TGF- β (left) in heart tissues from different groups, and the corresponding densitometric analysis (right). (B) mRNA expression of collagen I, α -SMA, and TGF- β (left) in heart tissues from different groups. (C) Representative images of stained longitudinal sections of LV tissue with picrosirius red (scale bar, 50 μ m) (top) and Masson (scale bar, 50 μ m) (bottom) from different groups, and the corresponding quantitative analysis of collagen deposition. (D) Protein expression of collagen I, α -SMA, and TGF- β (left) in cardiac fibroblasts from different groups, and the corresponding densitometric analysis (right). (E) mRNA expression of collagen I, α -SMA, and TGF- β in cardiac fibroblasts from different groups. (F) Protein expression of collagen I, α -SMA, and TGF- β (left) in cardiac fibroblasts from different groups, and the corresponding densitometric analysis (right). (G) mRNA expression of collagen I, α -SMA, and TGF- β (left) in cardiac fibroblasts from different groups, and the corresponding densitometric analysis (right). $n = 3$ per group, all mRNA and protein expression were normalized to GAPDH. The results are expressed as the mean \pm SEM (* $p < 0.05$, ** $p < 0.01$, *** $p < 0.001$, **** $p < 0.0001$).

rats was most significantly downregulated compared with those in the control group (Figure 1C). Also, we found NaCl could downregulate miR-142-3p expression in NRCFs (Figure 1D).

miR-142-3p participated in HSD-induced myocardial fibrosis and NaCl-induced cardiac fibrosis

In order to examine the role of miR-142-3p in HSD-induced myocardial fibrosis, the rats fed with CD or HSD were intravenously injected with 50 nM miR-142-3p agomiR or vehicle every 4 days. After verified miR-142-3p expression in heart tissues (Figure S2A), western blot (WB) and qPCR results showed that miR-142-3p agomiR administration prevented HSD-induced collagen I, α -SMA, and TGF- β expression in heart tissues (Figures 2A and 2B). The Masson's and Sirius Red staining of left ventricle (LV) tissues showed the same trend in the collagen deposition (Figure 2C). Next, the reversal experiments were then performed to investigate the role of miR-142-3p in NaCl-induced cardiac fibrosis in

NRCFs. After verified the efficiencies (Figure S2A), we found that miR-142-3p agomiR pretreatment prevented NaCl-induced collagen I, α -SMA and TGF- β expression (Figures 2D and 2E). Next, we incubated NRCFs with miR-142-3p agomiR to further investigate the role of miR-142-3p in the pro-fibrotic effects of NaCl treatment. After verified the efficiencies (Figure S2B), WB and qPCR results showed that miR-142-3p agomiR induced cardiac fibroblast activation (Figures 2F and 2G). Aforementioned results indicated that miR-142-3p did be involved in HSD-induced myocardial fibrosis and NaCl-induced cardiac fibrosis.

HSD-induced myocardial mitophagy *in vivo* and NaCl-induced cardiac mitophagy *in vitro*

Next, we performed transcriptome RNA sequencing on NC or miR-142-3p agomiR-treated NRCFs (Figure 3A). The Volcano plot and scatterplot visually showed 902 significantly upregulated and 376 significantly downregulated genes in miR-142-3p agomiR-treated NRCFs compared to the NC group (Figures 3B and 3C). Next, the hierarchical clustering heatmap clustered genes with similar expression patterns, which may have common functions or participate in common metabolic pathways and signaling pathways (Figure 3D). Further, we performed the gene ontology (GO) and Reactome pathways analyses of the differentially expressed genes (Figures 3E and 3F). The top 10 enriched terms of biological process (BP), cellular component (CC), molecular function (MF), and the top 20 enriched terms of Reactome pathways were shown in Figure. Among them, the differential genes were most enriched in “inflammatory response”, “innate immune response”, and “immune system” that have been confirmed to be highly related to autophagy.^{30,31}

We then examined the occurrence of mitophagy in HSD-induced rats' hearts. A higher LC3-II level was found in the HSD group than in the NC group (Figure 4A). The qPCR results revealed upregulated Beclin-1 and downregulated p62 mRNA expression in HSD-induced rats compared with that in the NC group (Figure 4B). Consistent with the previous observations, after HSD, increased autophagic vacuoles was found by the transmission electron microscopy (Figure 4C), indicating that the autophagic balance was disturbed. Besides, the levels of mitochondrial proteins (TOM20 for outer membrane, TIM23 for inner membrane) were reduced by HSD (Figure 4D), which collectively suggested that HSD may induce mitophagy *in vivo*.

In vitro, we found NaCl induced the ratio of LC3-II/LC3-I (Figure 4E), and changed mRNA expression of both Beclin-1 and p62 (Figure 4F). Moreover, the yellow dots with the merge of green (GFP) and red (mCherry) fluorescence signals, representing the formation of autophagosomes, were observed in the PBS group. After NaCl induction, distinct mCherry puncta covered the quenched green fluorescence, indicating the increased autophagic flux (Figure 4G). Besides, NaCl downregulated TOM20 and TIM23 protein expression (Figure 4H). The cells in the NaCl group showed higher reactivity for Annexin V-FITC and lower Mito-Tracker Red CMXRos fluorescence than those in the PBS group (Figure 4I), indicating that NaCl may influence cell viability and mitochondrial function.

miR-142-3p agomiR inhibited HSD-induced myocardial mitophagy and NaCl-induced cardiac mitophagy

Then, we investigated the role of miR-142-3p in HSD-induced myocardial mitophagy. The LC3-II levels were increased in LV tissues from rats in HSD group, which were attenuated by treating with miR-142-3p agomiR (Figure 5A). miR-142-3p agomiR administration also inhibited HSD-induced changes of Beclin-1 and p62 mRNA expression (Figure 5B). The numbers of autophagic vacuoles showed that miR-142-3p agomiR ameliorated HSD-induced autophagic flux in LV tissues (Figure 5C). Besides, decreased TOM20 and TIM23 protein expression detected in the LV tissues of HSD-induced rats were prevented by miR-142-3p agomiR administration (Figure S3A). Next, *in vitro*, NaCl-induced changed ratio of LC3-II/LC3-I, and mRNA expression of Beclin-1 and p62 were inhibited by miR-142-3p agomiR (Figures 5D and 5E). The fragmented mitochondria with distinct red puncta in NaCl-induced NRCFs was decreased by miR-142-3p agomiR (Figure 5G). Besides, deregulated TOM20 and TIM23 protein expression (Figure S3B), as well as the decreased stability of the membrane potential of NRCFs under NaCl environment were all attenuated by miR-142-3p agomiR (Figure 5G). Aforementioned results indicated that miR-142-3p agomiR inhibited HSD-induced myocardial mitophagy and NaCl-induced cardiac mitophagy.

miR-142-3p agomiR induced NaCl-induced cardiac mitophagy *in vitro*

Then, compared with the NC group, increased LC3-II/LC3-I ratio, upregulated Beclin-1, and downregulated p62 mRNA expression was found in the miR-142-3p agomiR group (Figures 6A and 6B). The increase of mCherry puncta and the decrease of GFP signal were observed in the NRCFs treated with miR-142-3p agomiR (Figure 6C). In addition, the cells in the miR-142-3p agomiR group showed lower TOM20 and TIM23 protein expression, and Mito-Tracker Red CMXRos fluorescence than those in the NC group (Figures 6D and 6E). Aforementioned results indicated that miR-142-3p did be involved in NaCl-induced cardiac fibrosis and mitophagy *in vitro*.

OPTN participated in miR-142-3p-mediated cardiac fibrosis and mitophagy in NaCl-induced NRCFs

OPTN was considered as an autophagy receptor for damaged mitochondria.³² Here, we found miR-142-3p agomiR significantly attenuated HSD or NaCl-induced OPTN mitochondrial protein expression *in vivo* or *in vitro*, respectively (Figures 7A and 7B). Also, miR-142-3p agomiR treatment upregulated OPTN expression *in vitro* (Figure S4A). In NaCl-induced NRCFs, increased OPTN puncta were observed within mitochondria (Figure 7C). In order to investigate the role of OPTN in miR-142-3p-mediated anti-fibrotic and anti-mitophagic effects, we incubated NaCl or PBS-treated NRCFs with si-OPTN. After verifying the efficiencies (Figure 7D), We found OPTN knockdown attenuated NaCl-induced protein and mRNA expression of collagen I, α -SMA, and TGF- β in NRCFs (Figures S5A and S5B). Si-OPTN dramatically prevented NaCl-induced autophagy in NRCFs (Figures 7E and 7F). As shown in Figures 7G–7I, NaCl-induced reduced TOM20 and TIM23 protein expression,

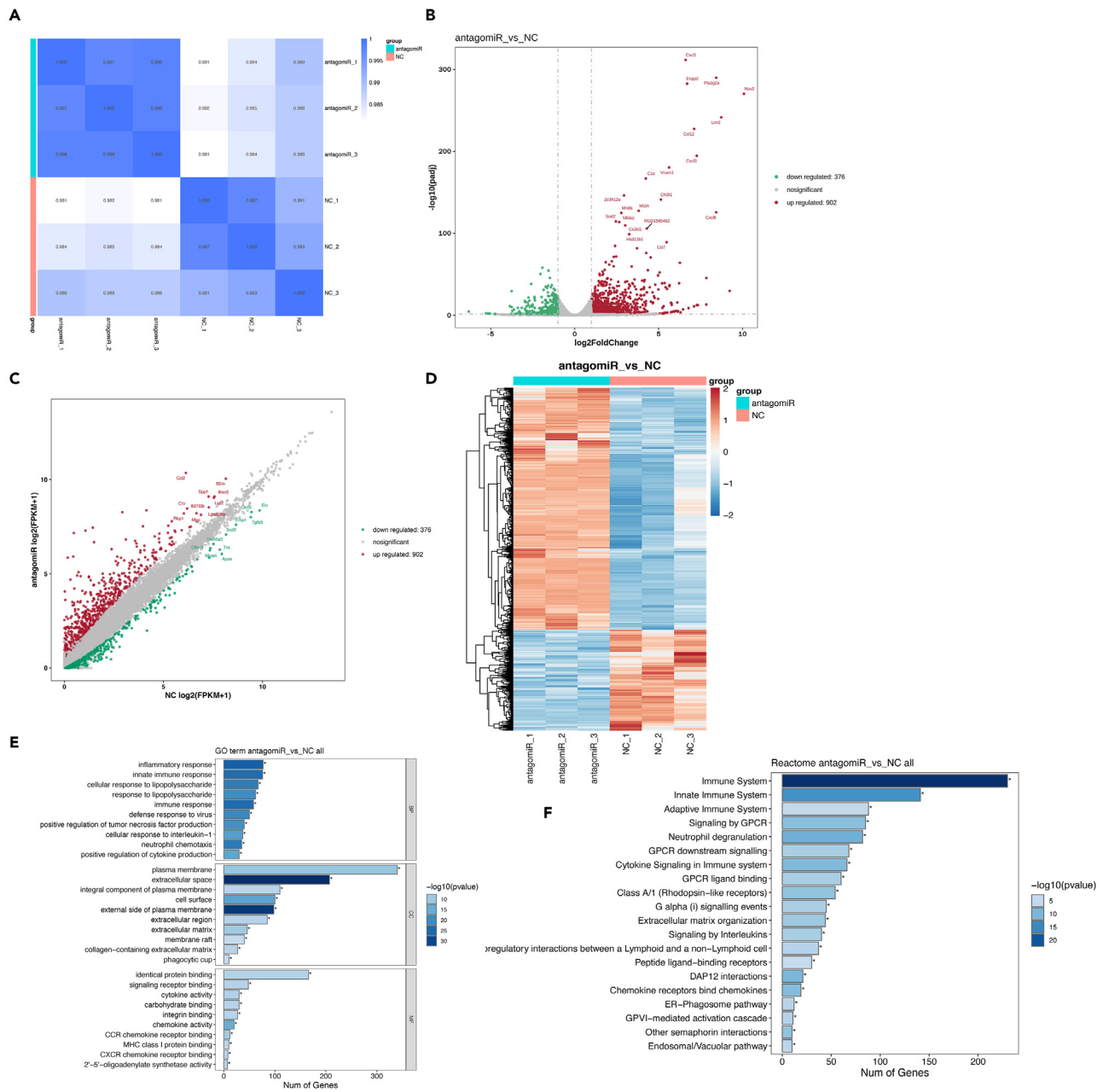


Figure 3. Functional analysis of differentially expressed genes

- (A) The correlation heatmap visually display differences between groups and sample duplication within groups.
 (B) The Volcano plot of differentially expressed genes among samples (FDR<0.01). Each point represents a gene.
 (C) The scatterplot of differentially expressed genes among samples.
 (D) The hierarchical clustering heatmap clustered genes with similar expression patterns.
 (E) The correlation GO analysis. The top 10 enriched terms of biological process, molecular function, and cellular component.
 (F) The Reactome pathways analysis of the differentially expressed genes.

decreased mitochondrial membrane potential, as well as increased cell apoptosis were inhibited by OPTN knockdown, indicating that suppression of OPTN ameliorated NaCl-induced cardiac fibroblast activation, and mitophagy *in vitro*.

Next, we incubated si-OPTN-treated NRCFs with miR-142-3p antagomiR. The WB and qPCR results showed that miR-142-3p antagomiR hampered the anti-fibrotic effects of si-OPTN on NaCl-induced NRCFs (Figures 8A and 8B). Also, the inhibitory effects of OPTN knockdown on NaCl-induced LC3-II/LC3-I ratio, and Beclin-1 mRNA expression were partially impeded by miR-142-3p antagomiR

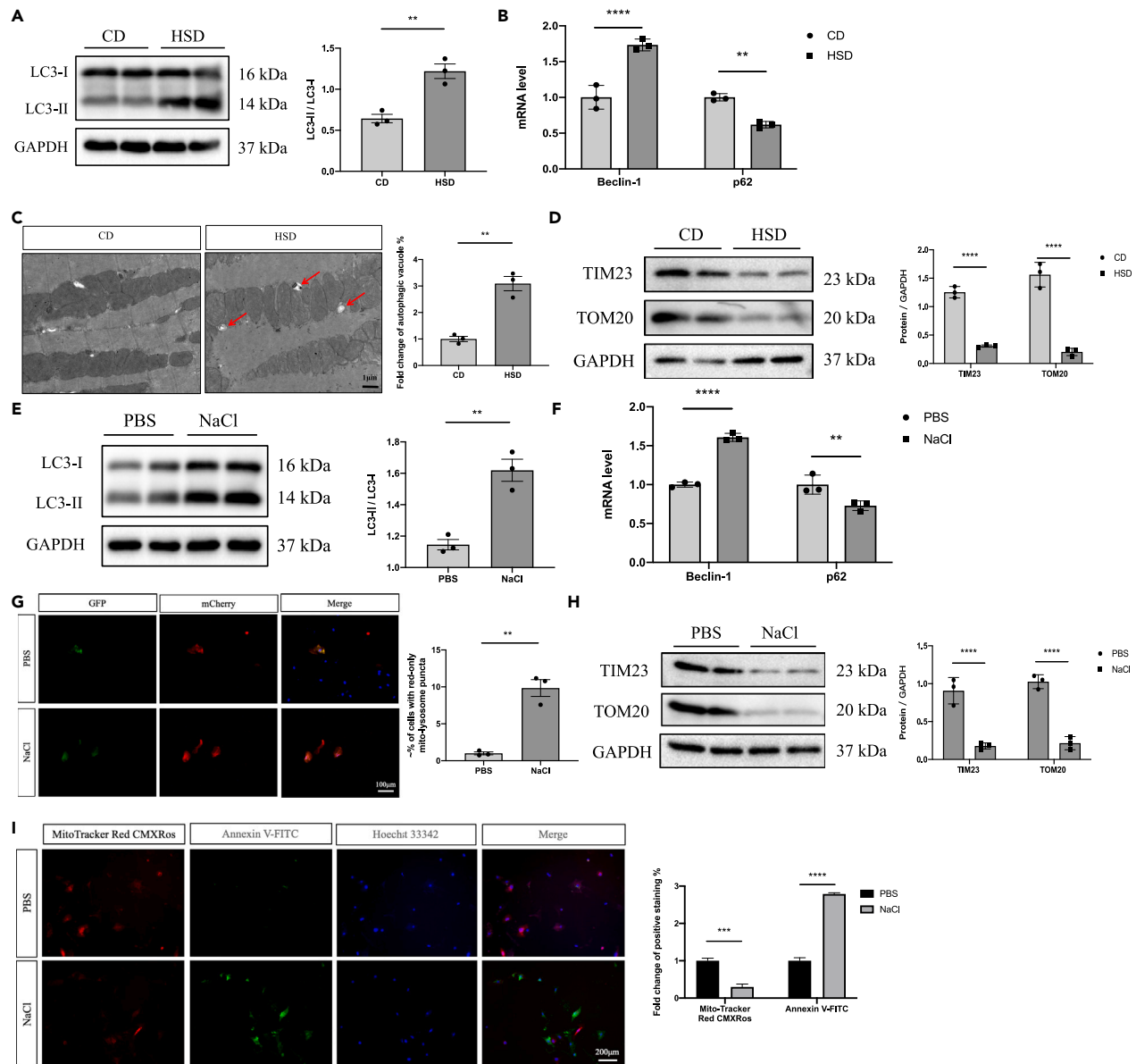


Figure 4. HSD-induced myocardial mitophagy *in vivo* and NaCl-induced cardiac mitophagy *in vitro*

(A) Protein expression of LC3 (left) in heart tissues from CD and HSD groups, and the corresponding densitometric analysis (right). (B) mRNA expression of Beclin-1, and p62 in heart tissues from CD and HSD groups. (C) The transmission electron microscopy showing autophagosomes (arrowhead) in heart tissues from CD and HSD groups. (D) Protein expression of TIM23, and TOM20 in heart tissues from CD and HSD groups (left), and the corresponding densitometric analysis (right). (E) Protein expression of LC3 (left) in cardiac fibroblasts from PBS and NaCl groups, and the corresponding densitometric analysis (right). (F) mRNA expression of Beclin-1, and p62 in heart tissues from PBS and NaCl groups. (G) Mitophagy in cardiac fibroblasts transfected with pCMV-mCherry-GFP-LC3B (left), and the corresponding quantification of the cells with red-only puncta (right). (H) Protein expression of TIM23, and TOM20 in cardiac fibroblasts from PBS and NaCl groups, and the corresponding densitometric analysis. (I) Cell viability and membrane potential detection of cardiac fibroblasts from PBS and NaCl groups, and the corresponding quantification analysis. $n = 3$ per group, all mRNA and protein expression were normalized to GAPDH. The results are expressed as the mean \pm SEM (** $p < 0.01$, *** $p < 0.001$, **** $p < 0.0001$).

(Figures 8C and 8D). A similar trend was also seen in the TOM20 and TIM23 protein expression and Mito-Tracker Red CMXRos fluorescence (Figures 8E and 8F). Consistently, OPTN participated in miR-142-3p-mediated cardiac fibrosis and mitophagy in NaCl-induced NRCFs.

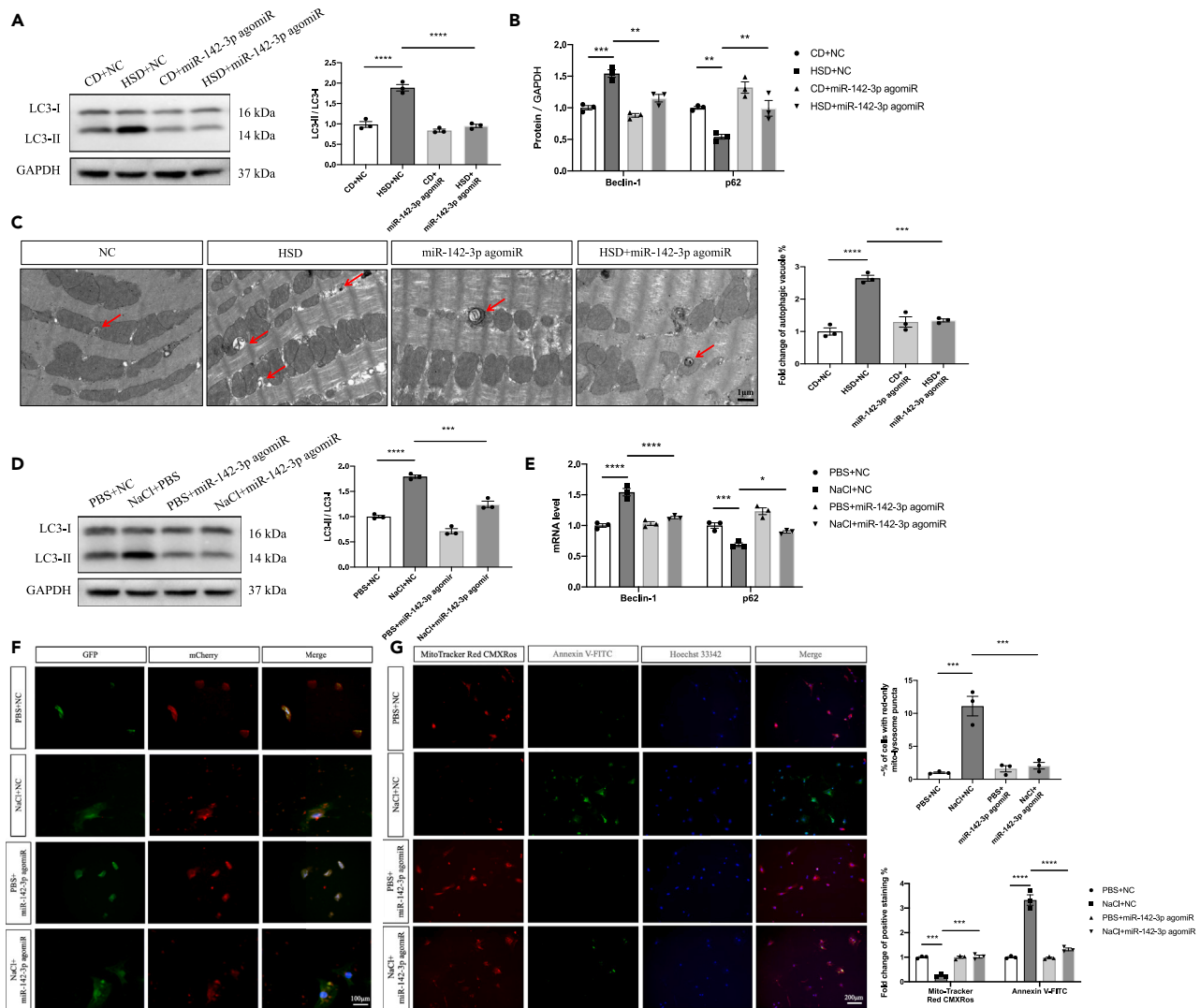


Figure 5. miR-142-3p agomiR inhibited HSD-induced myocardial mitophagy and NaCl-induced cardiac mitophagy

(A) Protein expression of LC3 (left) in heart tissues from different groups, and the corresponding densitometric analysis (right).

(B) mRNA expression of Beclin-1, and p62 in heart tissues different groups.

(C) The transmission electron microscopy showing autophagosomes (arrowhead) in heart tissues from different groups.

(D) Protein expression of LC3 (left) in cardiac fibroblasts from different groups, and the corresponding densitometric analysis (right).

(E) mRNA expression of Beclin-1, and p62 in heart tissues from different groups.

(F) Mitophagy in cardiac fibroblasts transfected with pCMV-mCherry-GFP-LC3B (left), and the corresponding quantification of the cells with red-only puncta (right).

(G) Cell viability and membrane potential detection of cardiac fibroblasts from different groups, and the corresponding quantification analysis. $n = 3$ per group, all mRNA and protein expression were normalized to GAPDH. The results are expressed as the mean \pm SEM (* $p < 0.05$, ** $p < 0.01$, *** $p < 0.001$, **** $p < 0.0001$).

DISCUSSION

The novel findings of this study were that fibrosis and mitophagy were elevated in the heart of mice fed with HSD. The expression of miR-142-3p was reduced in the heart of HSD mice, and upregulation of miR-142-3p alleviated cardiac fibrosis via downregulating OPTN-mediated mitophagy.

Accumulating evidence has shown that autophagy may be an attractive therapeutic target for cardiac diseases.³³ However, the level of autophagy is controversy in different cardiac fibrosis models. Autophagy in the heart was enhanced in diabetic cardiomyopathy-related cardiac fibrosis,³⁴ but was reduced in isoprenaline-induced myocardial fibrosis.³⁵ Besides, dynamic balance of mitochondria within cells, characterized by the reciprocating fusion and division of mitochondria, is necessary for the preservation of cellular performance by the active and

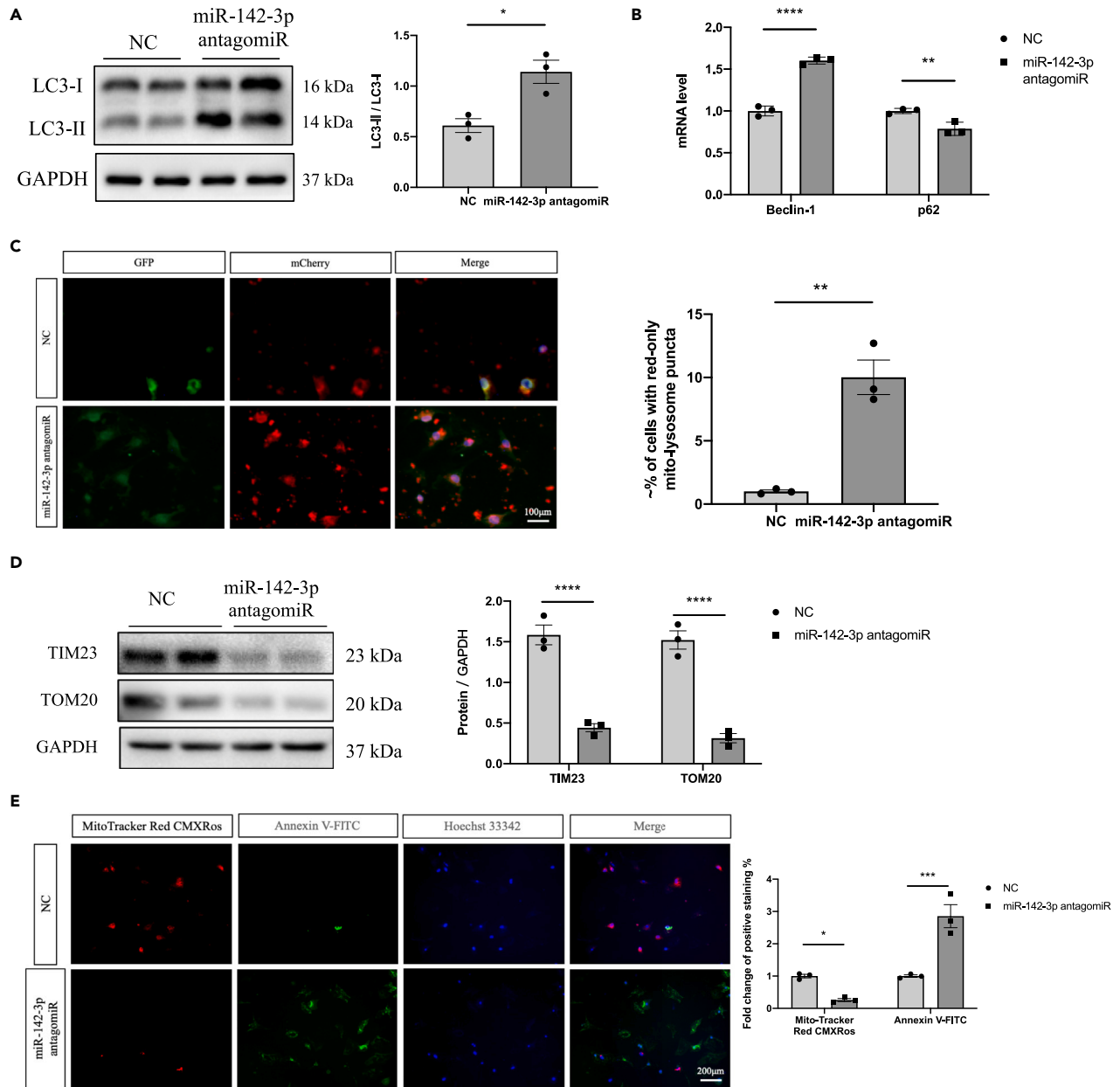


Figure 6. miR-142-3p antagoniR induced NaCl-induced cardiac mitophagy *in vitro*

(A) Protein expression of LC3 (left) in cardiac fibroblasts from different groups, and the corresponding densitometric analysis (right).

(B) mRNA expression of Beclin-1, and p62 in cardiac fibroblasts from different groups.

(C) Mitophagy in cardiac fibroblasts transfected with pCMV-mCherry-GFP-LC3B (left), and the corresponding quantification of the cells with red-only puncta (right).

(D) Protein expression of TIM23, and TOM20 in cardiac fibroblasts from different groups, and the corresponding densitometric analysis.

(E) Cell viability and membrane potential detection of cardiac fibroblasts from different groups, and the corresponding quantification analysis. $n = 3$ per group, all mRNA and protein expression were normalized to GAPDH. The results are expressed as the mean \pm SEM (* $p < 0.05$, ** $p < 0.01$, *** $p < 0.001$, **** $p < 0.0001$).

continuous response to external physiological or pathological stress.³⁶ Its imbalance may lead to the disorder of autophagy and other cellular processes,³⁷ resulting in the occurrence and progression of various diseases.³⁸ Mitophagy ensures cardiac homeostasis, which is essential for maintaining cardiac function.³⁹ We presently found that autophagy and mitophagy was increased in the heart of HSD rats, which was supported by our previous study.⁴

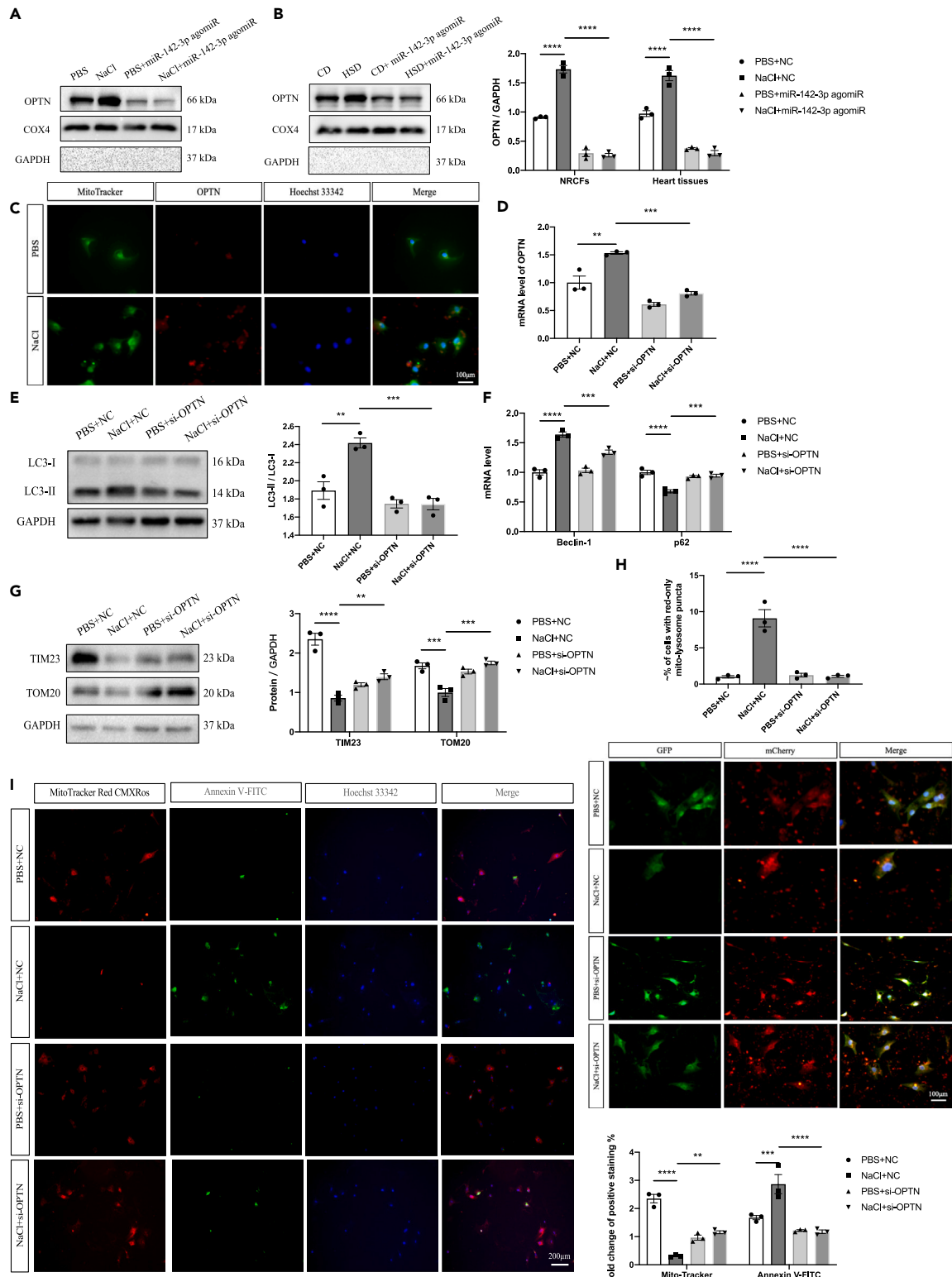


Figure 7. Suppression of OPTN ameliorated NaCl-induced cardiac fibroblast activation, and mitophagy *in vitro*

(A and B) Mitochondrial protein expression of OPTN in cardiac fibroblasts (A) or heart tissues (B) from indicated groups.
 (C) Co-localization of OPTN with mitochondria in cardiac fibroblasts from PBS and NaCl groups.
 (D) mRNA expression of OPTN in cardiac fibroblasts from different groups.
 (E) Protein expression of LC3 (left) in cardiac fibroblasts from different groups, and the corresponding densitometric analysis (right).
 (F) mRNA expression of Beclin-1, and p62 in cardiac fibroblasts from different groups.
 (G) Protein expression of TIM23, and TOM20 in cardiac fibroblasts from different groups, and the corresponding densitometric analysis.
 (H) Mitophagy in cardiac fibroblasts transfected with pCMV-mCherry-GFP-LC3B (left), and the corresponding quantification of the cells with red-only puncta (right).
 (I) Cell viability and membrane potential detection of cardiac fibroblasts from different groups, and the corresponding quantification analysis. $n = 3$ per group, all mRNA and protein expression were normalized to GAPDH or COX4. The results are expressed as the mean \pm SEM (* $p < 0.05$, ** $p < 0.01$, *** $p < 0.001$, **** $p < 0.0001$).

Since cardiac fibrosis and myocardium apoptosis were enhanced in HSD rats,^{4,5} multiple miRs in the heart were dysregulated after receiving HSD.^{5,40} We have previously reported that the upregulation of miR-210-5p could attenuate cardiac fibroblast activation in NRCFs via targeting TGFBR1.⁵ In this study, it was indeed that miR-142-3p expression in the heart tissues of HSD rats was significantly downregulated compared with those in the control group, as we reported previously.⁵ Previous studies have found the role of miR-142-3p in multiple cardiovascular diseases. AgomiR of miR-142-3p mitigates cardiac hypertrophy of rats induced by ligation of the abdominal aorta.²⁹ Also, miR-142-3p was significantly downregulated in coronary microembolization-induced myocardial injury.⁴¹ Moreover, injection miR-142 agomiR into mice and miR-142 mimic transfection in neonatal rat cardiomyocytes plays a role in protecting the heart from ischemia and reperfusion damage and malfunction.²⁵ We present found that the downregulation of miR-142-3p expression may result in cardiac fibrosis caused by HSD, which was supported by our next findings that administration of miR-142-3p antagomiR-induced cardiac fibrosis. In addition, miR-142-3p agomiR administration attenuated the fibrosis of heart in rats induced by HSD. These results indicated that miR-142-3p was dysregulated in the heart of HSD, and upregulation of miR-142-3p alleviated cardiac fibrosis.

In our study, we first found NaCl-induced differential genes were most enriched in the functional terms called “inflammatory response”, “innate immune response”, and “immune system”. The active cross talk exists between immune system and autophagy bolstered the significance of inflammatory response and immunological functions of autophagy in metabolic disorders, myopathies, cancers, and other diseases.^{30,42} The proven importance of autophagy revealed its crucial role in immunity and inflammation.^{15,43} As an essential, homeostatic process, autophagy has been recognized to be involved in key aspects of the immune response, which span both innate and adaptive immunity.⁴⁴ Also, the autophagy dysfunction could result in inflammatory diseases with hyperinflammation or/and excessive generation of mitochondria-generated reactive oxygen species.³¹ Thus, as a central fulcrum that balances the beneficial and harmful effects of immunity and inflammation, autophagy could be an attractive target in the treatment of related clinical diseases.

As a molecular switch between cell autophagy and apoptosis, miRNAs participate in the determination of cell fate via modulating transcription of target genes.^{45,46} Recent studies underlined the crucial transcriptional regulatory role of miRNA in almost all mitophagic pathways and mitophagic players or receptors of mitophagy.⁴⁷ The global view of the miRNA-mitophagy interconnection favored the design of miRNAs as effective therapeutic tools for manipulating autophagy under various pathological conditions.⁴⁷ In the current study, we found that miR-142-3p agomiR administration attenuated the increase of autophagy induced by HSD. The levels of mitochondrial outer membrane protein TOM20 and inner membrane protein TIM23⁴⁸ was reduced in the heart of HSD rats, which was reversed after miR-142-3p agomiR administration, indicating the importance of miR-142-3p in protection against cardiac fibrosis via attenuation of mitophagy. In addition, administration of miR-142-3p antagomiR increased mitophagy, which further supported the previous conclusion.

OPTN, a macroautophagy/autophagy receptor, is found to play a critical role in selective autophagy via phosphorylation by TBK1 (TANK-binding kinase 1).⁴⁹ As a mitophagy-associated protein, OPTN translocated to the damaged mitochondria during mitophagy, facilitating the engulfment of damaged organelles into phagophores, which is pivotal for mitochondrial clearance.⁵⁰ OPTN is associated with many human disorders that are closely related to autophagy, such as osteoporosis, rheumatoid arthritis, and nephropathy.⁵¹ However, the effects of OPTN in cardiovascular diseases were still not clear. We presently found that OPTN in the mitochondria of heart was increased after HSD treatment, and downregulation of OPTN alleviated high salt-induced heart fibrosis and autophagy. In addition, OPTN downregulation reversed miR-142-3p antagomiR-induced fibrosis and mitophagy. These results demonstrated that OPTN-mediated mitophagy enhanced the cardiac fibrosis induced by high salt.

Last, in our study, we had not focused on which target gene of miR-142-3p might be involved in its cardioprotective effects. However, the RNA-seq results indicated that the expression levels of several genes may be upregulated when miR-142-3p knock down (Figure S6A). WB and PCR results verified that miR-142-3p antagomiR or NaCl treatment significantly increased inducible nitric oxide synthase (NOS2) expression *in vitro* (Figures S6B and S6C). Th

e predictive tool further showed that NOS2 may be the target gene of miR-142-3p (Figure S7). Notably, NOS2 expression has been implicated in the cardiac dysfunction associated with cardiomyopathy, and cardiac remodeling.^{52,53} Here, we also found that silencing NOS2 ameliorated NaCl-induced cardiac fibrosis in NRCFs (Figure S6D). However, whether overexpression of miR-142-3p attenuated OPTN-mediated mitophagy via NOS2 remained to be explored.

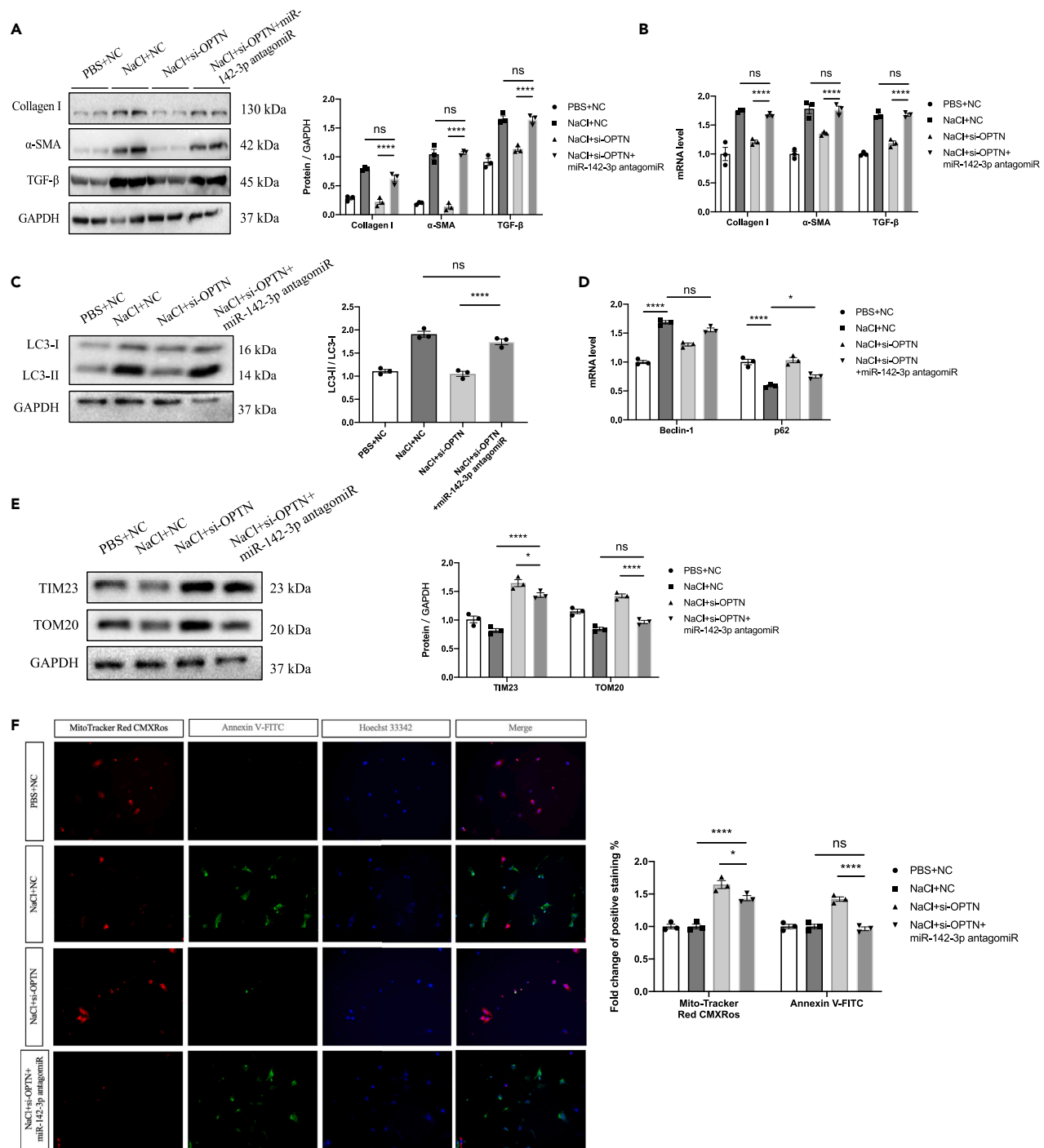


Figure 8. miR-142-3p antagoniR hampered the protective effects of si-OPTN on NaCl-induced NRCFs

(A) Protein expression of collagen I, α-SMA, and TGF-β (left) in cardiac fibroblasts from different groups, and the corresponding densitometric analysis (right). (B) mRNA expression of collagen I, α-SMA, and TGF-β (left) in cardiac fibroblasts from different groups. (C) Protein expression of LC3 (left) in cardiac fibroblasts from different groups, and the corresponding densitometric analysis (right). (D) mRNA expression of Beclin-1, and p62 in cardiac fibroblasts from different groups. (E) Protein expression of TIM23, and TOM20 in cardiac fibroblasts from different groups, and the corresponding densitometric analysis. (F) Cell viability and membrane potential detection of cardiac fibroblasts from different groups, and the corresponding quantification analysis. $n = 3$ per group, all mRNA and protein expression were normalized to GAPDH. The results are expressed as the mean \pm SEM (NS indicates not significant, * $p < 0.05$, ** $p < 0.01$, *** $p < 0.001$, **** $p < 0.0001$).

In conclusions, HSD-induced cardiac fibrosis via enhanced mitophagy. The expression of miR-142-3p was dysregulated in the heart of HSD rats. Upregulation of miR-142-3p could significantly alleviated high salt-induced cardiac fibrosis via attenuation of OPTN-mediated mitophagy.

Limitations of the study

First, although we found that OPTN-mediated mitophagy may explain the cardiac protective effects of miR-142-3p, further investigations should be performed to determine which target genes of miR-142-3p might be involved in this molecular pathway. Second, since we altered the miR-142-3p expression *in vivo* via caudal vein administration, more studies are needed to confirm whether this non-targeted organ administration has a positive or negative effect on kidney, blood vessel, and other organ damage caused by HSD. Third, concerning the safety of therapeutic targeting miRNAs, more preclinical and clinical research are needed to determine the possibility of targeted drug delivery, which may avoid the potential negative impacts caused by unknown targets of miRNAs.

STAR★METHODS

Detailed methods are provided in the online version of this paper and include the following:

- KEY RESOURCES TABLE
- RESOURCE AVAILABILITY
 - Lead contact
 - Materials availability
 - Data and code availability
- EXPERIMENTAL MODEL AND STUDY PARTICIPANT DETAILS
 - Animals
 - *In vivo* animal studies
 - Primary cell cultures
 - Cell transfection
- METHOD DETAILS
 - Masson and Picosirius red staining
 - RNA-sequencing (RNA-seq)
 - Western blotting
 - Quantitative real-time PCR (RT-qPCR)
 - High-throughput small RNA sequencing (sRNA-seq)
 - Transmission electron microscopy
 - Mitochondrial isolation
 - Mitochondrial membrane potential detection assay
- QUANTIFICATION AND STATISTICAL ANALYSIS

SUPPLEMENTAL INFORMATION

Supplemental information can be found online at <https://doi.org/10.1016/j.isci.2024.109764>.

ACKNOWLEDGMENTS

This work was supported by the industry prospecting and common key technology key projects of Jiangsu Province Science and Technology Department (grant no. BE2020721); Nanjing Life and Health Technology Special Project "Cooperative research, development and transformation of active intelligent health management platform for diabetes mellitus" (202205053); Industrial chain collaborative innovation Project of Ministry of Industry and Information Technology "Multi-modal medical data intelligent management software for the new generation of information technology" (TC210804V); the Industrial and Information Industry Transformation and Upgrading Special Fund of Jiangsu Province in 2021 (grant no. [2021]92); the Key Project of Smart Jiangsu in 2020 (grant no. [2021]1); Jiangsu Province Engineering Research Center of Big Data Application in Chronic Disease and Intelligent Health Service (grant no. [2020] 1460); Postdoctoral foundation of Jiangsu Province (2021K444C); the Youth Program of the National Natural Science Foundation of China (82300309); and the Jiangsu Funding Program for Excellent Postdoctoral Talent (2023ZB592).

AUTHOR CONTRIBUTIONS

Conceptualization, Yong Li and K.Z.; methodology, L.L. and Y.H.; analysis, F.Y. and P.L.; original draft writing, Yong Li and Yiu Liu; supervision and funding acquisition, Yiu Liu; review and editing, all authors.

DECLARATION OF INTERESTS

The authors declare no competing interests.

Received: August 4, 2023
Revised: October 23, 2023
Accepted: April 15, 2024
Published: April 17, 2024

REFERENCES

- Patel, Y., and Joseph, J. (2020). Sodium Intake and Heart Failure. *Int. J. Mol. Sci.* 21, 9474. <https://doi.org/10.3390/ijms21249474>.
- Xu, J., and Mao, F. (2022). Role of high-salt diet in non-alcoholic fatty liver disease: a mini-review of the evidence. *Eur. J. Clin. Nutr.* 76, 1053–1059. <https://doi.org/10.1038/s41430-021-01044-8>.
- Hunter, R.W., Dhaun, N., and Bailey, M.A. (2022). The impact of excessive salt intake on human health. *Nat. Rev. Nephrol.* 18, 321–335. <https://doi.org/10.1038/s41581-021-00533-0>.
- Li, Y., Wu, X., Mao, Y., Liu, C., Wu, Y., Tang, J., Zhao, K., and Li, P. (2021). Nitric Oxide Alleviated High Salt-Induced Cardiomyocyte Apoptosis and Autophagy Independent of Blood Pressure in Rats. *Front. Cell Dev. Biol.* 9, 646575. <https://doi.org/10.3389/fcell.2021.646575>.
- Zhao, K., Mao, Y., Ye, X., Ma, J., Sun, L., Li, P., and Li, Y. (2021). MicroRNA-210-5p alleviates cardiac fibrosis via targeting transforming growth factor-beta type I receptor in rats on high sodium chloride (NaCl)-based diet. *Eur. J. Pharmacol.* 912, 174587. <https://doi.org/10.1016/j.ejphar.2021.174587>.
- Robinson, A.T., Edwards, D.G., and Farquhar, W.B. (2019). The Influence of Dietary Salt Beyond Blood Pressure. *Curr. Hypertens. Rep.* 21, 42. <https://doi.org/10.1007/s11906-019-0948-5>.
- Wang, R., and Wang, G. (2019). Autophagy in Mitochondrial Quality Control. *Adv. Exp. Med. Biol.* 1206, 421–434. https://doi.org/10.1007/978-981-15-0602-4_19.
- Nah, J., Zablocki, D., and Sadoshima, J. (2021). The roles of the inhibitory autophagy regulator Rubicon in the heart: A new therapeutic target to prevent cardiac cell death. *Exp. Mol. Med.* 53, 528–536. <https://doi.org/10.1038/s12276-021-00600-3>.
- Xiong, R., Li, N., Chen, L., Wang, W., Wang, B., Jiang, W., and Geng, Q. (2021). STING protects against cardiac dysfunction and remodeling by blocking autophagy. *Cell Commun. Signal.* 19, 109. <https://doi.org/10.1186/s12964-021-00793-0>.
- Turkieh, A., El Masri, Y., Pinet, F., and Dubois-Deruy, E. (2022). Mitophagy Regulation Following Myocardial Infarction. *Cells* 11, 199. <https://doi.org/10.3390/cells11020199>.
- Luan, Y., Luan, Y., Feng, Q., Chen, X., Ren, K.D., and Yang, Y. (2021). Emerging Role of Mitophagy in the Heart: Therapeutic Potentials to Modulate Mitophagy in Cardiac Diseases. *Oxid. Med. Cell. Longev.* 2021, 3259963. <https://doi.org/10.1155/2021/3259963>.
- Forte, M., Bianchi, F., Cotugno, M., Marchitti, S., Stanzione, R., Maglione, V., Sciarretta, S., Valenti, V., Carnevale, R., Versaci, F., et al. (2021). An interplay between UCP2 and ROS protects cells from high-salt-induced injury through autophagy stimulation. *Cell Death Dis.* 12, 919. <https://doi.org/10.1038/s41419-021-04188-4>.
- Ryan, T.A., and Tumbarello, D.A. (2018). Optineurin: A Coordinator of Membrane-Associated Cargo Trafficking and Autophagy. *Front. Immunol.* 9, 1024. <https://doi.org/10.3389/fimmu.2018.01024>.
- Ying, H., and Yue, B.Y.J.T. (2016). Optineurin: The autophagy connection. *Exp. Eye Res.* 144, 73–80. <https://doi.org/10.1016/j.exer.2015.06.029>.
- Song, Y., Zhou, Y., and Zhou, X. (2020). The role of mitophagy in innate immune responses triggered by mitochondrial stress. *Cell Commun. Signal.* 18, 186. <https://doi.org/10.1186/s12964-020-00659-x>.
- Chen, K., Dai, H., Yuan, J., Chen, J., Lin, L., Zhang, W., Wang, L., Zhang, J., Li, K., and He, Y. (2018). Optineurin-mediated mitophagy protects renal tubular epithelial cells against accelerated senescence in diabetic nephropathy. *Cell Death Dis.* 9, 105. <https://doi.org/10.1038/s41419-017-0127-z>.
- Wang, Y., Zhu, J., Liu, Z., Shu, S., Fu, Y., Liu, Y., Cai, J., Tang, C., Liu, Y., Yin, X., and Dong, Z. (2021). The PINK1/PARK2/optineurin pathway of mitophagy is activated for protection in septic acute kidney injury. *Redox Biol.* 38, 101767. <https://doi.org/10.1016/j.redox.2020.101767>.
- Errington, N., Iremonger, J., Pickworth, J.A., Kariotis, S., Rhodes, C.J., Rothman, A.M., Condliffe, R., Elliot, C.A., Kiely, D.G., Howard, L.S., et al. (2021). A diagnostic miRNA signature for pulmonary arterial hypertension using a consensus machine learning approach. *EBioMedicine* 69, 103444. <https://doi.org/10.1016/j.ebiom.2021.103444>.
- Ghafouri-Fard, S., and Taheri, M. (2021). The expression profile and role of non-coding RNAs in obesity. *Eur. J. Pharmacol.* 892, 173809. <https://doi.org/10.1016/j.ejphar.2020.173809>.
- Ntelios, D., Georgiou, E., Alexouda, S., Malousi, A., Efthimiadis, G., and Zimargiorgis, G. (2022). A critical approach for successful use of circulating microRNAs as biomarkers in cardiovascular diseases: the case of hypertrophic cardiomyopathy. *Heart Fail. Rev.* 27, 281–294. <https://doi.org/10.1007/s10741-021-10084-y>.
- Wei, Y., Xiao, L., Yingying, L., and Haichen, W. (2022). Pinoresinol diglucoside ameliorates H/R-induced injury of cardiomyocytes by regulating miR-142-3p and HIF1AN. *J. Biochem. Mol. Toxicol.* 36, e23175. <https://doi.org/10.1002/jbt.23175>.
- Sharma, P., Yadav, P., Sundaram, S., Venkatraman, G., Bera, A.K., and Karunakaran, D. (2022). HMGB3 inhibition by miR-142-3p/sh-RNA modulates autophagy and induces apoptosis via ROS accumulation and mitochondrial dysfunction and reduces the tumorigenic potential of human breast cancer cells. *Life Sci.* 304, 120727. <https://doi.org/10.1016/j.lfs.2022.120727>.
- Xu, Y., Lv, X., Cai, R., Ren, Y., He, S., Zhang, W., Li, Q., Yang, X., Dai, R., Wei, R., and Su, Q. (2022). Possible implication of miR-142-3p in coronary microembolization induced myocardial injury via ATXN1L/HDAC3/NOL3 axis. *J. Mol. Med.* 100, 763–780. <https://doi.org/10.1007/s00109-022-02198-z>.
- Wang, Y., Ouyang, M., Wang, Q., and Jian, Z. (2016). MicroRNA-142-3p inhibits hypoxia/reoxygenation-induced apoptosis and fibrosis of cardiomyocytes by targeting high mobility group box 1. *Int. J. Mol. Med.* 38, 1377–1386. <https://doi.org/10.3892/ijmm.2016.2756>.
- Zhao, Z., Qu, F., Liu, R., and Xia, Y. (2020). Differential expression of miR-142-3p protects cardiomyocytes from myocardial ischemia-reperfusion via TLR4/NFκB axis. *J. Cell. Biochem.* 121, 3679–3690. <https://doi.org/10.1002/jcb.29506>.
- Liang, L., Fu, J., Wang, S., Cen, H., Zhang, L., Mandukhail, S.R., Du, L., Wu, Q., Zhang, P., and Yu, X. (2020). MiR-142-3p enhances chemosensitivity of breast cancer cells and inhibits autophagy by targeting HMGB1. *Acta Pharm. Sin.* B 10, 1036–1046. <https://doi.org/10.1016/j.apsb.2019.11.009>.
- Xiang, H., Yang, J., Li, J., Yuan, L., Lu, F., Liu, C., and Tang, Y. (2020). Citrate pretreatment attenuates hypoxia/reoxygenation-induced cardiomyocyte injury via regulating microRNA-142-3p/Rac1 axis. *J. Recept. Signal Transduct. Res.* 40, 560–569. <https://doi.org/10.1080/10799893.2020.1768548>.
- Su, Q., Liu, Y., Lv, X.W., Ye, Z.L., Sun, Y.H., Kong, B.H., and Qin, Z.B. (2019). Inhibition of lncRNA TUG1 upregulates miR-142-3p to ameliorate myocardial injury during ischemia and reperfusion via targeting HMGB1- and Rac1-induced autophagy. *J. Mol. Cell. Cardiol.* 133, 12–25. <https://doi.org/10.1016/j.yjmcc.2019.05.021>.
- Liu, B.L., Cheng, M., Hu, S., Wang, S., Wang, L., Tu, X., Huang, C.X., Jiang, H., and Wu, G. (2018). Overexpression of miR-142-3p improves mitochondrial function in cardiac hypertrophy. *Biomed. Pharmacother.* 108, 1347–1356. <https://doi.org/10.1016/j.biopha.2018.09.146>.
- Valdora, R., and Macian, F. (2012). Autophagy and the regulation of the immune response. *Pharmacol. Res.* 66, 475–483. <https://doi.org/10.1016/j.phrs.2012.10.003>.
- Ma, Y., Galluzzi, L., Zitvogel, L., and Kroemer, G. (2013). Autophagy and cellular immune responses. *Immunity* 39, 211–227. <https://doi.org/10.1016/j.immuni.2013.07.017>.
- Wong, Y.C., and Holzbaur, E.L.F. (2014). Optineurin is an autophagy receptor for damaged mitochondria in parkin-mediated mitophagy that is disrupted by an ALS-linked mutation. *Proc. Natl. Acad. Sci. USA* 111, E4439–E4448. <https://doi.org/10.1073/pnas.1405752111>.
- Wu, X., Liu, Z., Yu, X.Y., Xu, S., and Luo, J. (2021). Autophagy and cardiac diseases: Therapeutic potential of natural products. *Med. Res. Rev.* 41, 314–341. <https://doi.org/10.1002/med.21733>.
- Zhang, M., Sui, W., Xing, Y., Cheng, J., Cheng, C., Xue, F., Zhang, J., Wang, X., Zhang, C., Hao, P., and Zhang, Y. (2021). Angiotensin IV attenuates diabetic cardiomyopathy via suppressing FoxO1-induced excessive autophagy, apoptosis and fibrosis. *Theranostics* 11, 8624–8639. <https://doi.org/10.7150/thno.48561>.

35. Wang, L., Yuan, D., Zheng, J., Wu, X., Wang, J., Liu, X., He, Y., Zhang, C., Liu, C., Wang, T., and Zhou, Z. (2019). Chikusetsu saponin IVa attenuates isoprenaline-induced myocardial fibrosis in mice through activation autophagy mediated by AMPK/mTOR/ULK1 signaling. *Phytomedicine* 58, 152764. <https://doi.org/10.1016/j.phymed.2018.11.024>.
36. Wai, T., and Langer, T. (2016). Mitochondrial Dynamics and Metabolic Regulation. *Trends Endocrinol. Metabol.* 27, 105–117. <https://doi.org/10.1016/j.tem.2015.12.001>.
37. Whitley, B.N., Engelhart, E.A., and Hoppins, S. (2019). Mitochondrial dynamics and their potential as a therapeutic target. *Mitochondrion* 49, 269–283. <https://doi.org/10.1016/j.mito.2019.06.002>.
38. Brown, D.A., Perry, J.B., Allen, M.E., Sabbah, H.N., Stauffer, B.L., Shaikh, S.R., Cleland, J.G.F., Colucci, W.S., Butler, J., Voors, A.A., et al. (2017). Expert consensus document: Mitochondrial function as a therapeutic target in heart failure. *Nat. Rev. Cardiol.* 14, 238–250. <https://doi.org/10.1038/nrcardio.2016.203>.
39. Yang, M., Linn, B.S., Zhang, Y., and Ren, J. (2019). Mitophagy and mitochondrial integrity in cardiac ischemia-reperfusion injury. *Biochim. Biophys. Acta, Mol. Basis Dis.* 1865, 2293–2302. <https://doi.org/10.1016/j.bbadis.2019.05.007>.
40. Guo, T.S., Zhang, J., Mu, J.J., Liu, F.Q., Yuan, Z.Y., Ren, K.Y., and Wang, D. (2014). High-salt intake suppressed microRNA-133a expression in Dahl SS rat myocardium. *Int. J. Mol. Sci.* 15, 10794–10805. <https://doi.org/10.3390/ijms150610794>.
41. Su, Q., Lv, X., Ye, Z., Sun, Y., Kong, B., Qin, Z., and Li, L. (2022). Correction to: The mechanism of miR-142-3p in coronary microembolization-induced myocardial injury via regulating target gene IRAK-1. *Cell Death Dis.* 13, 85. <https://doi.org/10.1038/s41419-022-04546-w>.
42. Deretic, V. (2011). Autophagy in immunity and cell-autonomous defense against intracellular microbes. *Immunol. Rev.* 240, 92–104. <https://doi.org/10.1111/j.1600-065X.2010.00995.x>.
43. Levine, B., Mizushima, N., and Virgin, H.W. (2011). Autophagy in immunity and inflammation. *Nature* 469, 323–335. <https://doi.org/10.1038/nature09782>.
44. Deretic, V. (2005). Autophagy in innate and adaptive immunity. *Trends Immunol.* 26, 523–528. <https://doi.org/10.1016/j.it.2005.08.003>.
45. Xu, J., Wang, Y., Tan, X., and Jing, H. (2012). MicroRNAs in autophagy and their emerging roles in crosstalk with apoptosis. *Autophagy* 8, 873–882. <https://doi.org/10.4161/auto.19629>.
46. Ke, X., Liao, Z., Luo, X., Chen, J.Q., Deng, M., Huang, Y., Wang, Z., and Wei, M. (2022). Endothelial colony-forming cell-derived exosomal miR-21-5p regulates autophagic flux to promote vascular endothelial repair by inhibiting SIPL1A2 in atherosclerosis. *Cell Commun. Signal.* 20, 30. <https://doi.org/10.1186/s12964-022-00828-0>.
47. Strappazzon, F. (2020). A global view of the miRNA-mitophagy connexion. *Prog. Mol. Biol. Transl. Sci.* 172, 37–54. <https://doi.org/10.1016/bs.pmbts.2020.03.006>.
48. Nasoni, M.G., Carloni, S., Canonico, B., Burattini, S., Cesarini, E., Papa, S., Pagliarini, M., Ambrogini, P., Balduini, W., and Luchetti, F. (2021). Melatonin reshapes the mitochondrial network and promotes intercellular mitochondrial transfer via tunneling nanotubes after ischemic-like injury in hippocampal HT22 cells. *J. Pineal Res.* 71, e12747. <https://doi.org/10.1111/jpi.12747>.
49. Tschurtschenthaler, M., and Adolph, T.E. (2018). The Selective Autophagy Receptor Optineurin in Crohn's Disease. *Front. Immunol.* 9, 766. <https://doi.org/10.3389/fimmu.2018.00766>.
50. Evans, C.S., and Holzbaur, E.L.F. (2020). Lysosomal degradation of depolarized mitochondria is rate-limiting in OPTN-dependent neuronal mitophagy. *Autophagy* 16, 962–964. <https://doi.org/10.1080/15548627.2020.1734330>.
51. Qiu, Y., Wang, J., Li, H., Yang, B., Wang, J., He, Q., and Weng, Q. (2022). Emerging views of OPTN (optineurin) function in the autophagic process associated with disease. *Autophagy* 18, 73–85. <https://doi.org/10.1080/15548627.2021.1908722>.
52. Lin, J.R., Ding, L.L.Q., Xu, L., Huang, J., Zhang, Z.B., Chen, X.H., Cheng, Y.W., Ruan, C.C., and Gao, P.J. (2022). Brown Adipocyte ADRB3 Mediates Cardioprotection via Suppressing Exosomal iNOS. *Circ. Res.* 131, 133–147. <https://doi.org/10.1161/circresaha.121.320470>.
53. Dawood, A.F., Alzamil, N.M., Hewett, P.W., Momenah, M.A., Dallak, M., Kamar, S.S., Abdel Kader, D.H., Yassin, H., Haidara, M.A., Maarouf, A., and Al-Ani, B. (2022). Metformin Protects against Diabetic Cardiomyopathy: An Association between Desmin-Sarcomere Injury and the iNOS/mTOR/TIMP-1 Fibrosis Axis. *Biomedicines* 10, 984. <https://doi.org/10.3390/biomedicines10050984>.

STAR★METHODS

KEY RESOURCES TABLE

REAGENT or RESOURCE	SOURCE	IDENTIFIER
Antibodies		
TOM20 Monoclonal antibody	Proteintech Co.	Cat No: 66777-1-Ig; RRID: AB_2882123
Tim23 Polyclonal antibody	Proteintech Co.	Cat No: 11123-1-AP; RRID: AB_615045
LC3 Polyclonal antibody	Proteintech Co.	Cat No: 14600-1-AP; RRID: AB_2137737
TGF Beta Polyclonal antibody	Proteintech Co.	Cat No: 21898-1-AP; RRID: AB_2811115
smooth muscle actin Polyclonal antibody	Proteintech Co.	Cat No: 14395-1-AP; RRID: AB_2223009
Collagen Type I Polyclonal antibody	Proteintech Co.	Cat No: 14695-1-AP; RRID: AB_2082037
iNOS Polyclonal antibody	Proteintech Co.	Cat No: 22226-1-AP; RRID: AB_2879038
OPTN Polyclonal antibody	Proteintech Co.	Cat No: 10837-1-AP; RRID: AB_2156665
COXIV Polyclonal antibody	Proteintech Co.	Cat No: 11242-1-AP; RRID: AB_2085278
GAPDH antibody	Beyotime Co.	Cat No: AF0006; RRID: AB_2107448
Bacterial and virus strains		
miR-142-3p agomiR	RiboBio Co.	N/A
pCMV-mCherry-GFP-LC3B	Beyotime Co.	Cat No: D2816
Chemicals, peptides, and recombinant proteins		
TRIzol Reagent	Thermo Fisher Scientific	Cat. No. 15596026
High salt diet	Research Diets Inc.	Cat. No. A10008
glutaraldehyde	Sigma-Aldrich Co.	Cat. No. 111-30-8
Osmium Acid	Sigma-Aldrich Co.	Cat. No. 20816-12-0
EPON 812 resin	Sigma-Aldrich Co.	Cat. No. 25134-21-8
collagenase type II	Worthington Biochemical Corp.	Cat. No. 9001-12-1
pancreatin	Sigma-Aldrich Co.	Cat. No. 8049-47-6
Lipofectamine RNAiMAX	Invitrogen	Cat. No. 13778030
Critical commercial assays		
Pierce BCA Protein Assay Kit	Thermo Fisher Scientific	Cat No. 23225
Masson staining kit	Beyotime Co.	Cat No. C0189S
PrimeScript™ RT reagents kit	TaKaRa Biomedical Technology	Cat No. RR037B
mitochondrial extraction kit	Solarbio	Cat No. SA1020
Mitochondrial Membrane Potential Detection Kit	Beyotime Co.	Cat No. C1071
Deposited data		
RNA-seq data	GEO repository	https://www.ncbi.nlm.nih.gov/geo/query/acc.cgi?acc=GSE262000
sRNA-seq data	Mendeley	https://data.mendeley.com/datasets/9gm3vn6rz4/1
Original western blot	Mendeley	https://data.mendeley.com/datasets/r6p9wvnsn6j/1
Experimental models: Cell lines		
neonatal rat cardiac fibroblasts (NRCFs)	This paper	N/A
Experimental models: Organisms/strains		
Sprague-Dawley (SD) rats	Vital River Biological Co.	Male

(Continued on next page)

Continued

REAGENT or RESOURCE	SOURCE	IDENTIFIER
Oligonucleotides		
See Table S1 for all Primer sequences	This paper	N/A
Software and algorithms		
GraphPad Prism	GraphPad Software Inc Prism	https://www.graphpad.com/scientificsoftware/prism/ , RRID: SCR_002798
Image-Pro Plus software	Media Cybernetics, Inc.	https://imagej.nih.gov/ij/

RESOURCE AVAILABILITY

Lead contact

Further information and requests for resources and reagents should be directed to and will be fulfilled by the lead contact, Yong Li (liyongmydream@126.com).

Materials availability

This study did not generate new unique reagents.

Data and code availability

- RNA-seq data have been deposited at GEO and are publicly available as of the date of publication. Accession numbers are listed in the [key resources table](#). sRNA-seq data have been deposited at Mendeley and are publicly available as of the date of publication. The DOI is listed in the [key resources table](#). Original western blot images have been deposited at Mendeley and are publicly available as of the date of publication. The DOI is listed in the [key resources table](#). Microscopy data reported in this paper will be shared by the [lead contact](#) upon request.
- This paper does not report original code.
- Any additional information required to reanalyze the data reported in this paper is available from the [lead contact](#) upon request.

EXPERIMENTAL MODEL AND STUDY PARTICIPANT DETAILS

Animals

The rats were kept in a temperature-controlled room on a 12-h light-dark cycle with free access to standard chow and tap water. Approved by the Experimental Animal Care and Use Committee of Nanjing Medical University, all procedures were conducted in accordance with the Guide for the Care and Use of Laboratory Animals (NIH publication No. 85-23, revised in 1996). The experiments were carried out using male Sprague-Dawley (SD) rats weighing 160–180 g (Vital River Biological Co., Ltd, Beijing, China), and were randomly divided into the control diet (CD, 0.4% NaCl) group and the HSD (8% NaCl, Research Diets Inc., NJ, USA) group and fed for 8 weeks.

In vivo animal studies

Rats with CD or HSD were intravenously injected with 1 mL miR-142-3p agomiR (50 nM) or negative control (NC; 50 nM) every 5 days (RiboBio, Guangzhou, China). 30 days later, rats were anesthetized with isoflurane (3.5%) and sacrificed, and the hearts were collected for the further experiments.

Primary cell cultures

Primary neonatal rat cardiac fibroblasts (NRCFs) were isolated from 1- to 2-day-old newborn SD rats (Vital River Biological Co., Ltd.). Briefly, the heart was excised and digested through agitations in buffer containing collagenase type II (Worthington Biochemical Corp., NJ, USA) and pancreatin (Sigma, MO, USA). The atria and great vessels were discarded. The ventricles were cut into small pieces and digested with collagenase type II and pancreatin. Cells from digestion were collected, cultured in complete Dulbecco's modified Eagle's medium (DMEM; Biochannel Biotechnology Co., Ltd.) for 2-4 h to allow for the preferential attachment of CFs. Then, the medium containing cardiomyocytes were removed to enrich CFs. The CFs were cultured at 37°C with 5% CO₂ and 95% air. CFs that reached 70%–80% confluency were incubated in the serum-free DMEM medium for overnight starvation. Then, the cells were incubated with 100 mM NaCl for 24 h to induce the pathological phenotype.⁵

Cell transfection

The pCMV-mCherry-GFP-LC3B plasmid was obtained from Beyotime Biotechnology company (Shanghai, China). The short interfering RNA (siRNA) of OPTN, miR-142-3p agomiR, or antagomiR were synthesized from RiboBio company (Shanghai, China). CFs (5 × 10⁵) were seeded for

12 h at 37°C and 5% CO₂. Next, transfection procedures were carried out when the cells were 50% confluent. Briefly, 50 nM siRNA of OPTN, miR-142-3p agomiR or antagomiR was transfected into CFs using Lipofectamine RNAiMAX (Invitrogen, Carlsbad, CA, USA) following the manufacturers' instructions. After 6-8-h transfection, the medium was replaced with 10% FBS/DMEM for 12 h. Then, the cells underwent NaCl treatment upon 12-h starvation.

METHOD DETAILS

Masson and Picrosirius red staining

Cardiac sections (5 μm) were examined by Masson and Picrosirius red staining (Service Biological Technology Co., Ltd, Wuhan, China) according to the manufacture instruments to measure the fibrosis of cardiomyocytes. Three to five random fields were selected from each of three sections from each animal for observation under a light microscope (Carl Zeiss GmbH, Oberkochen, Germany). Images were analyzed using Image-Pro Plus software (Media Cybernetics, Inc., MD, USA).

RNA-sequencing (RNA-seq)

RNA-seq was performed from NRCFs that received miR-142-3p antagomiR or NC antagomiR treatment (3 biological repeats per group) by Biomarker Technologies Co., Ltd (Beijing, China). Briefly, U-mRNAseq Library Prep Kit for Illumina Novaseq 6000 was used for library preparation according to the instructions. First, mRNA was enriched using Oligo(dT) Beads after the extracted RNA samples has undergone strict quality control. Next, the mRNA was broken into short fragments. These short fragments were used as templates for cDNA synthesis with random primers. Suitable fragments were extracted and amplified by PCR to construct a cDNA library. After that, the insert size and the effective concentration of the cDNA libraries were quantified. Then, the prepared libraries were sequenced on an Illumina NovaSeq 6000 platform according to a PE 150 bp protocol. The clean reads for subsequent analysis were obtained after raw data filtering, sequencing error rate checking and GC content distribution checking. The clean reads were assembled into genome or transcriptome via Hisat2 software. Differential gene expression analysis was performed using the DESeq2 R-package (p -value>0.05, $|\log_2\text{Foldchange}|>1$). We last adopt clusterProfiler software to select widely-used annotated gene databases (Gene Ontology (GO), Kyoto Encyclopedia of Genes and Genomes (KEGG) and Reactome) for pathway enrichment analysis of differential genes.

Western blotting

Heart tissues or cultured cells were sonicated in RIPA lysis buffer and homogenized. The debris was removed and the supernatant was obtained after centrifugation at 12,000 g for 10 min at 4°C. About 30–50 μg proteins was loaded for electrophoresis, and probed with primary antibodies against collagen I (1:1000; No.14695-1-AP; Proteintech Co., Wuhan, China), α-SMA (1:1000; No.14395-1-AP; Proteintech Co.), TGF-β (1:1000; No.21898-1-AP; Proteintech Co.), LC3 I/II (1:1000; No.14600-1-AP; Proteintech Co., Wuhan, China), TIM23 (1:1000; No.11123-1-AP; Proteintech Co., Wuhan, China), TOM20 (1:1000; No.66777-1-Ig; Proteintech Co., Wuhan, China), OPTN (1:1000; No.10837-1-AP; Proteintech Co., Wuhan, China), COX4 (1:1000; No.11242-1-AP; Proteintech Co., Wuhan, China). GAPDH (1:1000, AF0006; Beyotime Biotechnology Co., Shanghai, China) was used as internal control. Images were analyzed using the Image-Pro Plus software.

Quantitative real-time PCR (RT-qPCR)

The total RNA in samples was extracted with TRIzol (Ambion, TX, USA). Next, the RNA was reverse transcribed into cDNA using PrimeScript RT reagents kit (TaKaRa Biomedical Technology, Beijing, China) in a total volume of 10 μL which contained 0.5 μg RNA, 2 μL 5×PrimeScript RT Master Mix, and RNase-free ddH₂O (up to 10 μL). The reaction conditions were processed at 37°C for 15 min, followed by 5 s at 85°C. All cDNA was stored at –80°C before use. mRNA was determined with SYBR Green I fluorescence. All samples were amplified in triplicates for 40 cycles in 384-well plates. The relative gene mRNA expression was expressed as 2^{-ΔΔCt}. The primers (Genscript, Nanjing, China) are shown in [Table S1](#). Bulge-loop miRNA qRT-PCR Primer Sets (one RT primer and a pair of qPCR primers for each set) specific for miR-142-5p was designed by RiboBio. U6 was normalization of miRNA expression.

High-throughput small RNA sequencing (sRNA-seq)

High-throughput sRNA-seq was performed from NRCFs that received NaCl or PBS treatment (3 biological repeats per group) by Biomarker Technologies Co., Ltd. In brief, the RNA extracted from samples were quantified and qualified to meet the requirements. Sequencing libraries were generated using NEBNextR UltraTM small RNA Sample Library Prep Kit for IlluminaR (NEB, USA) following manufacturer's recommendations and index codes were added to attribute sequences to each sample. Last, the libraries were sequenced on the Agilent Bioanalyzer 2100 platform (Illumina) and raw reads were generated. The raw data were then processed through in-house perl scripts to obtain the high-quality clean reads. The functional pathway enrichment analysis of the target genes with differentially expressed microRNA (miRNA) were implemented using clusterProfiler R packages.

Transmission electron microscopy

Heart tissue samples were immersed in a solution of 2.5% glutaraldehyde overnight at 4°C. After washing with phosphate buffer, samples were post-fixed in a 1% osmium acid for 2 h at 4°C. After two washes with ddH₂O, samples were stained in 2% uranyl acetate for 2 h, dehydrated in increasing concentration of ethanol, and infiltrated with 100% acetone for 2 h and EPON 812 resin overnight. Then, hearts were

polymerized at 37°C for 12 h, 45°C for 12 h and 60°C for 48 h. Thin sections of 70 nm were obtained and analyzed on a transmission electron microscope (FEI Tecnai G2 Spirit Bio TWIN).

Mitochondrial isolation

The mitochondria were extracted using the mitochondrial extraction kit (Solarbio), according to manufacturer's protocol. Briefly, the collected cells were homogenized in ice lysis buffer with a dounce glass homogenizer. Next, the homogenate was centrifuged at 1000×g for 10 min at 4°C for 3 times. Following that, the supernatant without pellet cell debris and nuclei was collected and then was centrifuged at 12,000×g at 4°C for 10 min to pellet mitochondria.

Mitochondrial membrane potential detection assay

The cell viability and membrane potential were detected in cardiac fibroblasts from different groups with a Mitochondrial Membrane Potential Detection Kit (C1071; Beyotime, Shanghai, China). Briefly, 50,000 cells were collected and then resuspended with 188 μL Annexin V-FITC. After that, the cells were incubated with the mixed solution containing 2 μL Mito-Tracker Red CMXRos, and 5 μL Annexin V-FITC for 30 min at room temperature in the dark. The stained cells were observed using a confocal laser scanning microscope (Carl Zeiss, Oberkochen, Germany).

QUANTIFICATION AND STATISTICAL ANALYSIS

Data were presented as mean ± standard error of the mean (SEM). The statistical significance among multiple groups was evaluated by one-way analysis of variance (ANOVA) with the Bonferroni post-hoc test. A two-tailed *p*-value <0.05 was considered statistically significant. **p* < 0.05, ***p* < 0.01, ****p* < 0.001, *****p* < 0.0001.